JOURNAL OF SOLID STATE CHEMISTRY 120, 279–289 (1995)

Synthesis and Structure of a New Oxycarbonate, $Sr_5Mn_4CO_3O_{10}$, Closely Related to the Perovskite Structure

V. Caignaert, B. Domengès, and B. Raveau

Laboratoire CRISMAT-ISMRA, Bd. Maréchal Juin, 14050 Caen Cedex, France

Received February 21, 1995; in revised form July 14, 1995; accepted July 20, 1995

A new strontium manganese oxycarbonate $Sr_5Mn_4CO_3O_{10}$, related to the perovskite structure, was synthesised, using solid state reaction. The mean structure of this compound was solved by X-ray diffraction and electron microscopy in the *P4/m* space group. The cell parameters are related to the perovskite cell a_p by the relation $a = a_p*\sqrt{5} = 8.795$ Å and $c = a_p = 3.785$ Å. This original phase can be deduced from the stoichiometric perovskite $SrMnO_3$, by removing one $[MnO_5]_\infty$ row of MnO_6 octahedra out of five, in an ordered way; this leads to the framework Mn_4O_{10}, built up from corner-sharing MnO_5 pyramids, forming tunnels which are in fact fully occupied by carbonate groups. The compound is antiferromagnetic with a Néel temperature $T_N = 260$ K. © 1995 Academic Press, Inc.

INTRODUCTION

The recent synthesis of superconducting copper oxycarbonates has shown the great ability of the CO_3 groups to accommodate the perovskite structure. A large series of phases such as $(Sr, Ba)_2CuO_2CO_3$ (1, 3), $A_{1-x}M_xSr_4Cu_2CO_3O_7$ with A = Hg,Tl and M = Bi, Pb (4–6), $TlSr_{4-x}Ba_xCu_2CO_3O_7$ (7), and $(Y, Ca)_n(Ba, Sr)_{2n}Cu_{3n-1}CO_3O_{7n-3}$ (8, 10) have indeed been isolated and characterized. In all these compounds the CO_3 groups share two of their apices either with CuO_6 octahedra or with CuO_5 pyramids, so that the perovskite layers are interconnected through rows of carbonate groups. Copper seems to be the only transition element that forms oxycarbonates with a mixed framework of corner-sharing CO_3 and CuO_5 or CuO_6 polyhedra. The difficulty in realizing such frameworks may be due to the great rigidity of the triangular CO_3 groups that impose O–C–O angles of 120° and C–O distances of 1.2–1.3 Å. Such an effect is compensated in the case of copper by the Jahn–Teller effect of Cu^{II} that allows rather flexible apical Cu–O distances in the CuO_6 octahedra and in the CuO_5 pyramids. In this respect, Mn^{III} is a potential candidate for the formation of oxycarbonates, owing to its d^4 electronic configuration that implies a Jahn–Teller distortion, leading to the formation of MnO_5 pyramids or MnO_6 octahedra. For this reason, the possibility of introducing carbonate groups in the Sr–Mn–O system has been investigated. We report herein on the first oxycarbonate $Sr_5Mn_4CO_3O_{10}$ with a structure closely related to perovskite.

SYNTHESIS

The exploration of the system $SrO–SrCO_3–Mn_2O_3$ was carried out from various mixtures of SrO, $SrCO_3$, MnO_2, and Mn, intimately ground in an agate mortar. Owing to its hydrolysis properties SrO was first prepared by decomposing SrO_2 and then stored in a glove box. The mixtures of SrO, $SrCO_3$, MnO_2, and Mn were ground, placed in an alumina crucible and finally sealed in an evacuated silica tube. These mixtures were heated at 1100°C for 24 hr. From the powder X-ray diffraction analysis, performed with a Guinier camera, it appears that a pure phase, with a pattern closely related to that of the perovskite, was isolated for the nominal composition $Sr_5(Mn_4CO_3)O_{10}$.

It is worth pointing out that this phase is often observed in the study of the system Sr–Mn–O due to an incomplete decarbonation of $SrCO_3$, or to a recarbonation of the products during the grinding step in air. For instance, with the reaction of $SrCO_3$ and MnO_2 in air at 800°C, followed by reaction of the resulting products with metallic manganese in an evacuated ampoule at 1100°C one observes significant formation of the oxycarbonate.

INFRARED MEASUREMENT

The IR spectrum was recorded over the frequency range 400–4000 cm^{-1} on a Nicolet 720 spectrometer using a pellet with a mixture of 2 mg sample in 100 mg of KBr. The spectrum provide sharp ν_2 and ν_3 characteristic modes of the CO_3^{2-} ion (at 864 and 1427 cm^{-1}, respectively). The ν_1 mode is not IR active and the ν_4 mode is not clearly identified. It is to be noted that these features, indicating a D_{3h} or (D_3) symmetry of the carbonate ion in $Sr_5Mn_4CO_3O_{10}$,

0022-4596/95 $12.00

are not compatible with the spectrum of the strontianite precursor ($SrCO_3$).

X-RAY DIFFRACTION AND HREM STUDY

The powder X-ray pattern of $Sr_5Mn_4CO_3O_{10}$ was registered with a Philips diffractometer using the Cu$K\alpha$ radiation from 9° to 135° (2θ) in steps of 0.02°. The manganese fluorescence was reduced by a graphite back-scattering monochromator. The data were refined with the program Fullprof (Version 2.6.2 (11)). For the electron microscopy study, the powder was gently ground in an agate mortar in *n*-butanol and deposited on a holey carbon-coated copper grid. The electron diffraction (ED) was performed on a JEM200CX equipped with a tilting rotating goniometer, which allows the reciprocal space reconstruction, and the high resolution study was performed on a TOPCON 2B electron microscope equipped with a ±10° double-tilt goniometer and an objective lens with a spherical aberration constant of 0.4 mm. High-resolution images (HREM) were simulated using the multislice method of the EMS package.

The indexation of the powder X-ray diffraction pattern (Fig. 1) and the ED observations allow the tetragonal symmetry to be evidenced, with absence of extinction conditions, leading to the possible space groups $P4$, $P\bar{4}$, $P4/m$, $P422$, $P4mm$, $P\bar{4}2m$, $P\bar{4}m2$, $P4/mmm$. The (001) ED pattern (Fig. 2) emphasises the cell relationships with the perovskite-type cell. Indeed, the intense dots of the pattern correspond to the ⟨110⟩-type reflections of the perovskite. The **a*** direction is parallel to the reciprocal [210]p* and the number of dots between the 000 and the 420p reflection gives the relation $a \approx a_p\sqrt{5}$. Besides the evidence of good

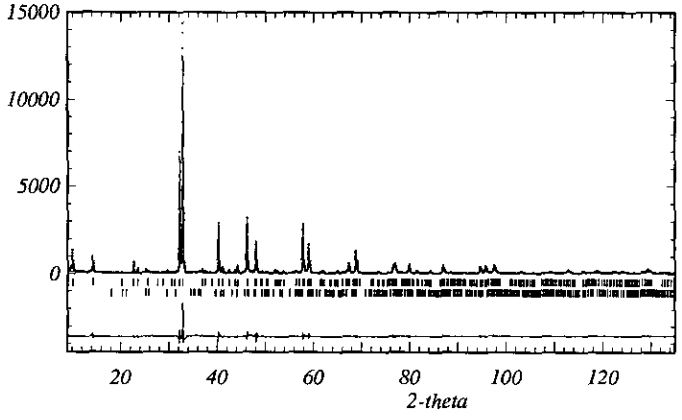

FIG. 1. Rietveld refinement profile of the X-ray powder diffraction data for $Sr_5Mn_4CO_3O_{10}$ (R_{wp} = 14.3%, R_{exp} = 7.8%, R_I = 6.1%). The observed intensities are shown by dots and the calculated ones by the solid line. The positions of the Bragg reflections for $Sr_5Mn_4CO_3O_{10}$ and $SrCO_3$ are shown by small vertical lines below the pattern. The line in the bottom indicates the intensity difference between the experimental and the refined pattern. The first Bragg peak is not refined because, at this angle, the cross section of the sample is lower than the X-ray beam dimensions.

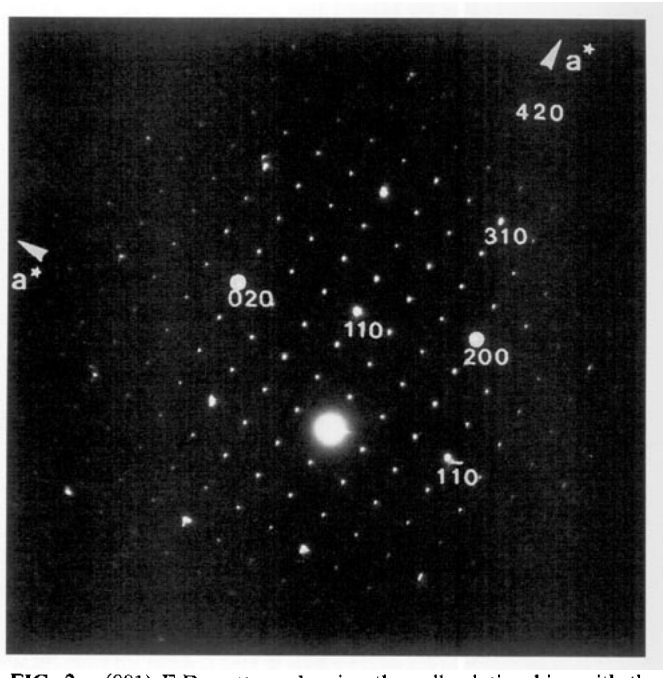

FIG. 2. (001) E.D. pattern showing the cell relationships with the perovskite-type subcell. Stronger dots are indexed in the perovskite cell.

crystallinity of the sample, many slightly rotated domains were detected through the presence of split dots forming arcs on E.D. patterns.

On this basis, the XRPD pattern was indexed in a tetragonal cell with a = 8.795 Å, c = 3.785 Å. The refinement of the structure was initiated in the space group $P4/m$. The origin of the cell was chosen on a strontium site and the structure was based on a B-deficient perovskite model with the cation positions

Sr_1	0, 0, 0
Sr_2	$x = 0.2, y = 0.4, 0$
Mn	$x = 0.3, y = 0.1, 1/2.$

After the refinement of the cation positions, a Fourier difference synthesis was undertaken. In the $P4/m$ space group, the *hkl* and *khl* peaks do not have the same structure factors and are superimposed on the powder pattern. So the powder profile refinement is unable to obtain an accurate observed structure factors for these couples of peaks and the data are biased by the structure model refined by the Rietveld method. In spite of this problem, the oxygen positions around the manganese atoms were easily obtained from the Fourier difference maps; these maps allow the identification of ten residuals with three oxygen sites, labeled O_1, O_2, and O_3. These oxygen sites lead to a pyramidal coordination for the manganese, which is compatible with the preferential coordination of the trivalent manganese. After the refinement of these cation and oxygen

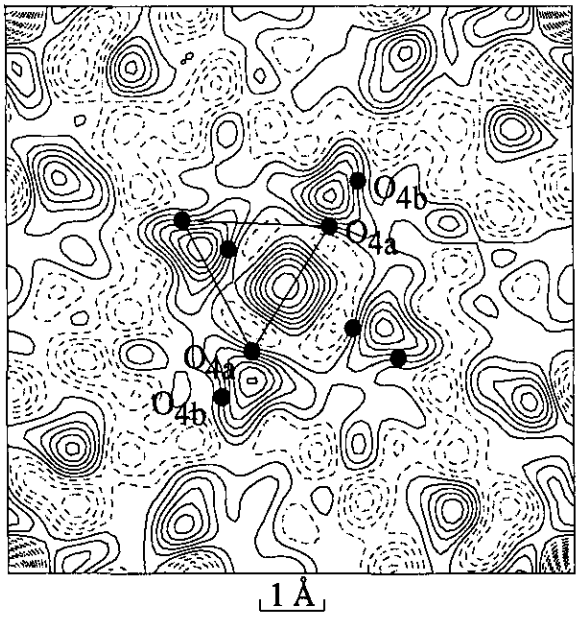

FIG. 3. Fourier difference at $z = 1/2$ along **c** for $Sr_5Mn_4CO_3O_{10}$ ($P4/m$) after the refinement of the strontium, manganese, and oxygen positions. The position of O_{4a} and O_{4b} oxygen sites are indicated by black dots.

positions, the reliability factors were lowered to $R_{wp} = 21\%$ ($\chi^2 = 7.2$) and $R_I = 14.1\%$ for the formula $Sr_5Mn_4O_{10}$. A subsequent Fourier difference revealed a fourfold residual at $z = 1/2$ around the center of the cell (Fig. 3), which can be attributed to the presence of the CO_3 groups. The distance of 2.25 Å between two O_{4a} peaks (Fig. 3), corresponds indeed exactly to the O–O distance in the CO_3 groups, so that one edge of the carbonate group may be directed along the [210] or the [120] direction. At this stage, two limit models can be considered for the orientation of the CO_3 group. In the first model, the plane of the CO_3 group is parallel to (001) so that there exists four possible orientations of the CO_3 groups within this plane, that correspond to the triangles $O_{4a}O_{4a}O_{4b'}$, and $O_{4a'}O_{4a'}O_{4b}$ in Fig. 3. In the second model the plane of the CO_3 groups is parallel to **c**, leading also to four possible orientations. The elongated shape of the peaks (couples $O_{4a}O_{4b}$ or $O_{4a'}O_{4b'}$) in the Fourier difference map, that allows "O_3" triangles with the right O–O distances to be drawn (Fig. 3), is strongly in favor of the first model. In contrast, no peak is observed at $z = 0.02$ or 0.98, so that the second limit model appears as less probable.

Taking into account the small impurity phase $SrCO_3$, in the Rietveld refinement, both models were tested. The best result was obtained with the O_4 oxygen positions at $x \approx 0.43$, $y \approx 0.39$, and $z = 1/2$. The reliability factors were significantly lowered to $R_{wp} = 15.8\%$ and $R_I = 6.1\%$. The final atomic coordinates are given in Table 1. Note that the abnormally high thermal factor of O_4, as well as the standard deviations on the coordinates, indicated that this site should be split into two different sites; this is in agreement with the Fourier difference map, which evidences an elongation of the residuals, interpreted as two atomic positions for oxygen, labelled O_{4a} and O_{4b} with an occupancy factor twice lighter for O_{4b} than for O_{4a} positions. Carbon has been located arbitrarily at the barycenter of the "O_3" triangle, and no refinement has been performed owing to its low scattering factor.

For HREM study, the [001] observation direction was chosen as most representative of the structure and, as expected from the [001] structure projection (Fig. 4a), the Mn sites substituted with carbonate CO_3 groups should be easily imaged. Indeed, experimental through-focus images show that most focus values allow the carbonates ions to be distinguished from the manganese and strontium ions (Fig. 5) in agreement with image calculations, based on the refined structural parameters; at focus 10 nm, carbonate groups are related to very bright dots forming a square 0.88×0.88 nm^2 array, whereas strontium and manganese atoms appear as gray ones spaced by 0.27 nm, i.e., $a_p/\sqrt{2}$ and along [130], one can count 9 gray dots between two bright ones; at −20 nm focus value, low electron densities are highlighted and oxygen atoms of the predicted structure appear as bright dots spaced by 0.27 nm, the four oxygen positions shared by carbon and neighbor manganese are those highlighted in a grayish disk related to carbonate location; at −50 focus value, high electron densities are highlighted and only strontium and manganese atoms appear as bright dots, whereas carbonate groups appear as slightly gray disks. These observations support strongly the XRD results. Indeed, they confirm that the strontium ions occupy the A sites of the stoichiometric

TABLE 1
Refined Structural Parameters for $Sr_5Mn_4CO_3O_{10}$ at Room Temperature

Site		x	y	z	B	Occ.
Sr_1	1a	0	0	0	0.50(9)	1
Sr_2	4j	0.1783(2)	0.3886(3)	0	0.66(3)	4
Mn	4k	0.3009(4)	0.0983(5)	1/2	0.43(5)	4
O_1	4j	0.3156(12)	0.1284(14)	0	1.1(2)	4
O_2	2f	1/2	0	1/2	1.1(4)	2
O_3	4k	0.1078(14)	0.2032(14)	1/2	0.8(3)	4
C	1d	1/2	1/2	1/2	0.7(4)	1
O_4	4k	0.430(4)	0.390(4)	1/2	6.8(8)	3
C	*4k*	*0.437*	*0.537*	*1/2*	—	*1*
O_{4a}	*4k*	*0.430*	*0.390*	*1/2*	—	*2*
O_{4b}	*4k*	*0.310*	*0.621*	*1/2*	—	*1*

Note. The theoretical positions for the carbonate group with plane parallel to (001) are given in italic. Cell parameters: $a = 8.7949(2)$ Å, $c = 3.7848(1)$ Å. Space group: $P4/m$. Reliability factors: $R_p = 10.5\%$, $R_{wp} = 14.3\%$, $R_e = 7.8\%$, $\chi^2 = 3.4$, $R_I = 6.1\%$.

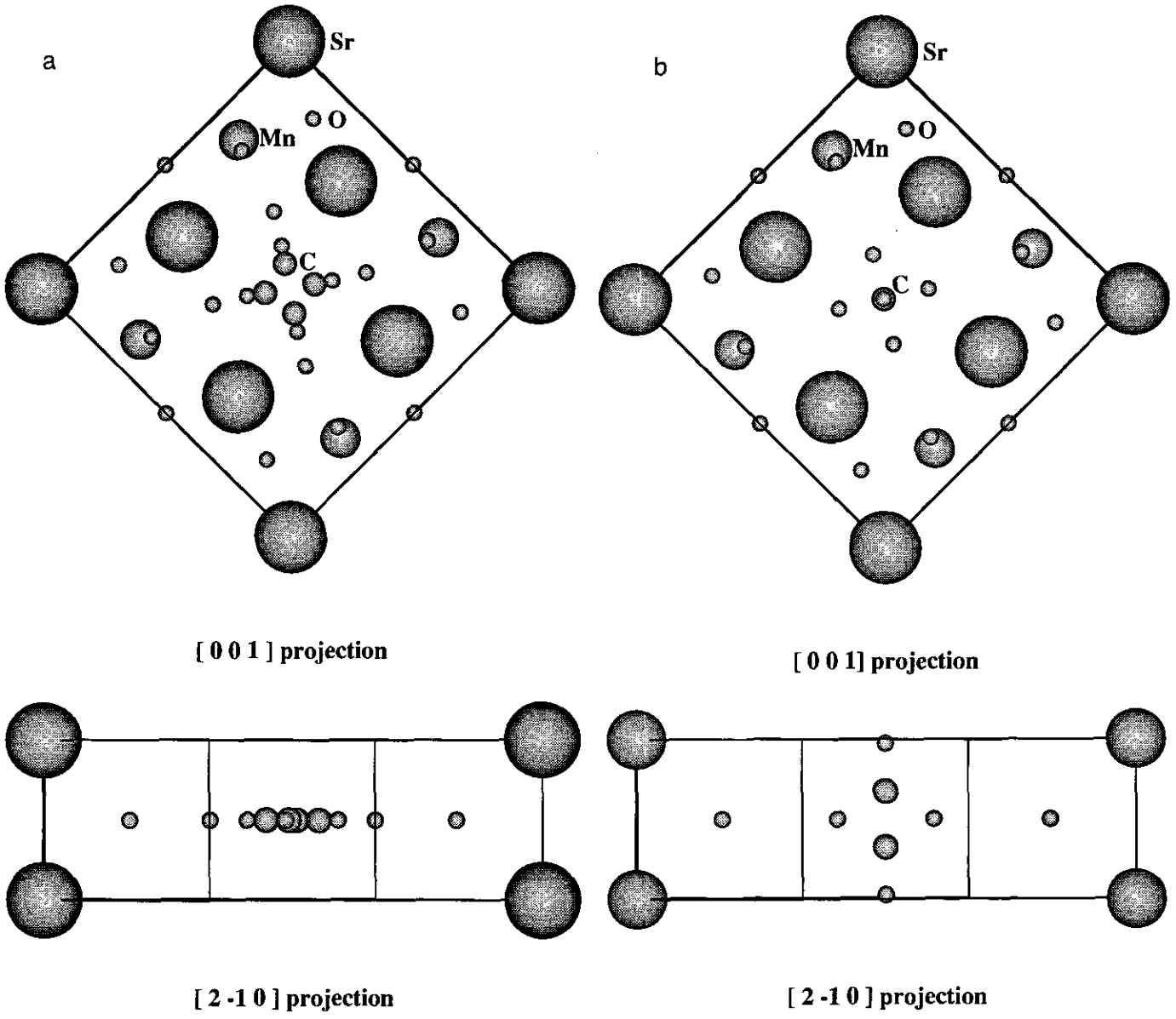

FIG. 4. [001] and [2 −1 0] projections of (a) $Sr_5Mn_4CO_3O_{10}$ structure, carbonate group is perpendicular to [001], and (b) model II structure, carbonate group is parallel to [001].

perovskite ABO_3, whereas the B sites are occupied by manganese and carbonate groups in an ordered manner. In order to confirm the orientation of the CO_3 plane proposed from XRD results, further image calculations were performed based on model II with the CO_3 plane perpendicular to (001) (Fig. 4b). In the second model C was located at $x = y = 1/2$ and $z = 0.675$, keeping two oxygens of the CO_3 groups in the positions $x \approx y \approx 0.4$ and $z = 1/2$, whereas the third oxygen was located at $x = y = 1/2$, $z = 0.02$, in order to get a regular CO_3 group. The calculated images (Fig. 6) show slight differences in contrast between the two models for definite focus values, even for thicknesses as low as 0.76 nm. This is particularly the case with the −20 nm and −50 nm focus values for which the calculated images of model I (Fig. 6a) show better agreement with the experimental images than those of model II (Fig. 6b).

Finally, it is worth pointing out that a weak residual has also been detected on the Fourier difference series at 1/2 1/2 1/2 (Fig. 3), which is not compatible with the carbon position deduced from the carbonate group geometry. This phenomenon, which could be explained by the presence of very small amounts of manganese in the structure, will be discussed later with the HREM study of defects.

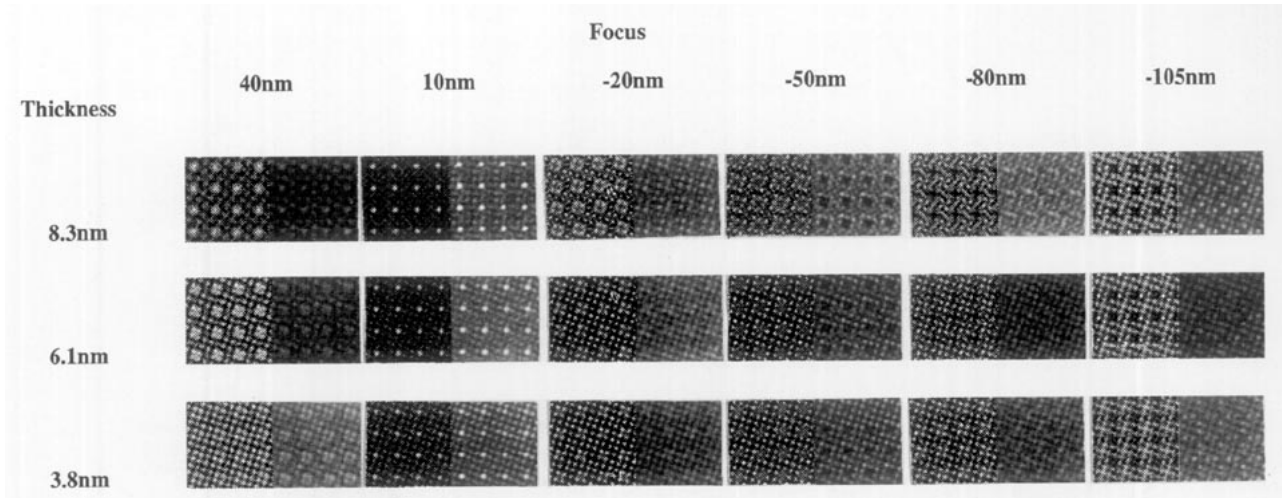

FIG. 5. $Sr_5Mn_4CO_3O_{10}$ calculated and experimental (001) through focus series, based on the refined structure parameters.

STRUCTURE DESCRIPTION

The above XRD and HREM study shows that the structure of the oxycarbonate $Sr_5Mn_4CO_3O_{10}$ is closely related to that of the "ideal cubic" perovskite $SrMnO_3$. As shown from Fig. 7a it consists of an oxygen-deficient perovskite $Sr_5Mn_4O_{10}$ built up from corner-sharing MnO_5 pyramids; the latter is deduced from the stoichiometric perovskite structure by removing one infinite row of MnO_6 octahedra out of five in an ordered way. In this respect, the Mn_4O_{10} framework exhibits a great analogy with the $La_4BaCu_5O_{13}$ structure (11) that is also characterized by similar groups of corner-sharing CuO_5 pyramids but differs from the manganese phase by the introduction of CuO_6 octahedra. But the most striking feature of this oxycarbonate deals with the presence of large tunnels which are in fact fully occupied by carbonate groups (Fig. 7b) with a plane parallel to (001). It is worth pointing out that each carbonate group forms with the MnO_5 pyramids two strongly distorted MnO_6 octahedra and one almost-regular MnO_6 octahedron, so that the structure should be described as an assemblage of MnO_5 pyramids and MnO_6 octahedra. Moreover, the orientation of the CO_3 groups is such that each strontium ion is surrounded by seven oxygen atoms belonging to MnO_5 pyramids and two oxygen atoms belonging to almost two different CO_3 groups, so that a strongly distorted tricapped trigonal prismatic SrO_9 polyhedron is formed.

Note that the CO_3 groups are presumed to be oriented at random in four different ways (Fig. 7c). Their orientation may indeed vary either in the same tunnel or from one tunnel to the other.

The interatomic distances deduced from the XRD calculations are listed in Table 2. The O_1, O_2, and O_3 sites correspond to the apices of the MnO_5 pyramids of the Mn_4O_{10} framework. They form four equatorial Mn–O distances ranging from 1.91 to 1.95 Å, and one longer apical Mn–O distance of 2.01 Å, in perfect agreement with the Jahn–Teller behaviour of Mn^{III}. The O_4 sites correspond to the refined positions of oxygens that form two apices of the CO_3 group; they should in fact be split according to the Fourier difference map into two sites (O_{4a} and O_{4b} positions, Fig. 3). For this reason a second site labeled O_{4b}, (coordinates $x = 0.310$, $y = 0.621$, and $z = 1/2$) is considered. Clearly, it appears that from the presence of the CO_3 groups, manganese at one time exhibits a sixth neighbor, O_{4a} at 2.80 Å, forming a very distorted octahedron, and at another time exhibits a sixth neighbor, O_{4b} at about 1.98 Å, forming an almost regular octahedron, always compatible with the Jahn–Teller effect of Mn^{III}. The strontium atoms Sr_1 located in the perovskite cages

TABLE 2
Selected Interatomic Distances (Å) of $Sr_5Mn_4CO_3O_{10}$

Sr_1–O_1	3.00(1)	×4
Sr_1–O_3	2.77(1)	×8
Sr_2–O_1	2.59(1)	×1
Sr_2–O_2	2.77(1)	×1
Sr_2–O_1	2.64(1)	×1
Sr_2–O_2	2.65(1)	×2
Sr_2–O_3	2.57(1)	×2
Sr_2–O_{4a}	2.91–3.10	[a]
Sr_2–O_{4b}	2.68–3.02	[a]
Mn–O_1	1.915(2)	×2
Mn–O_2	1.953(4)	×1
Mn–O_3	1.93(1)	×1
Mn–O_3	2.01(1)	×1
Mn–O_{4a}	2.80(4)	[a]
Mn–O_{4b}	1.98(4)	[a]

[a] These values depend on the carbonate orientation.

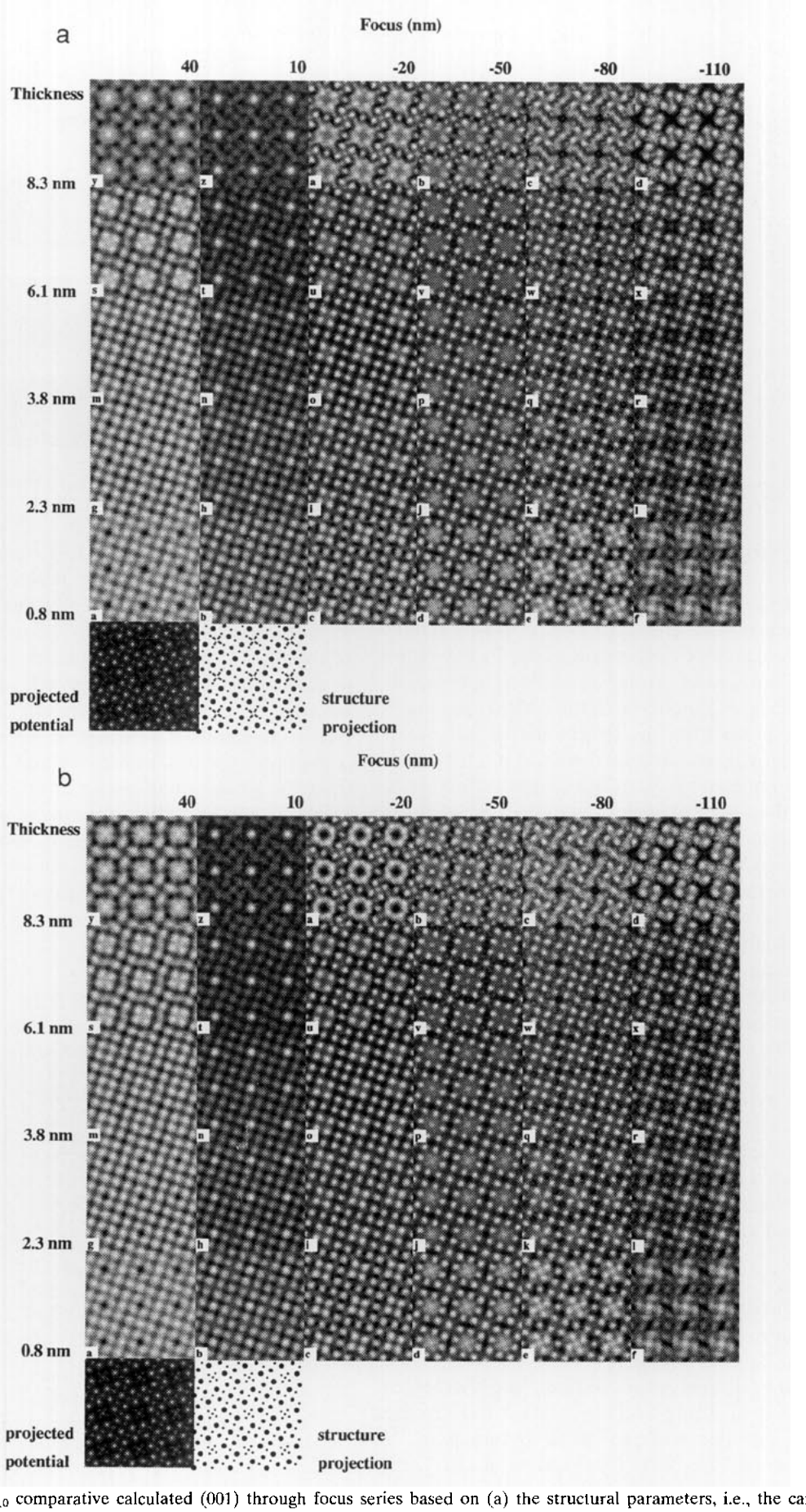

FIG. 6. $Sr_5Mn_4CO_3O_{10}$ comparative calculated (001) through focus series based on (a) the structural parameters, i.e., the carbonate groups parallel to (001), and (b) a structural model with the carbonate groups parallel to [001].

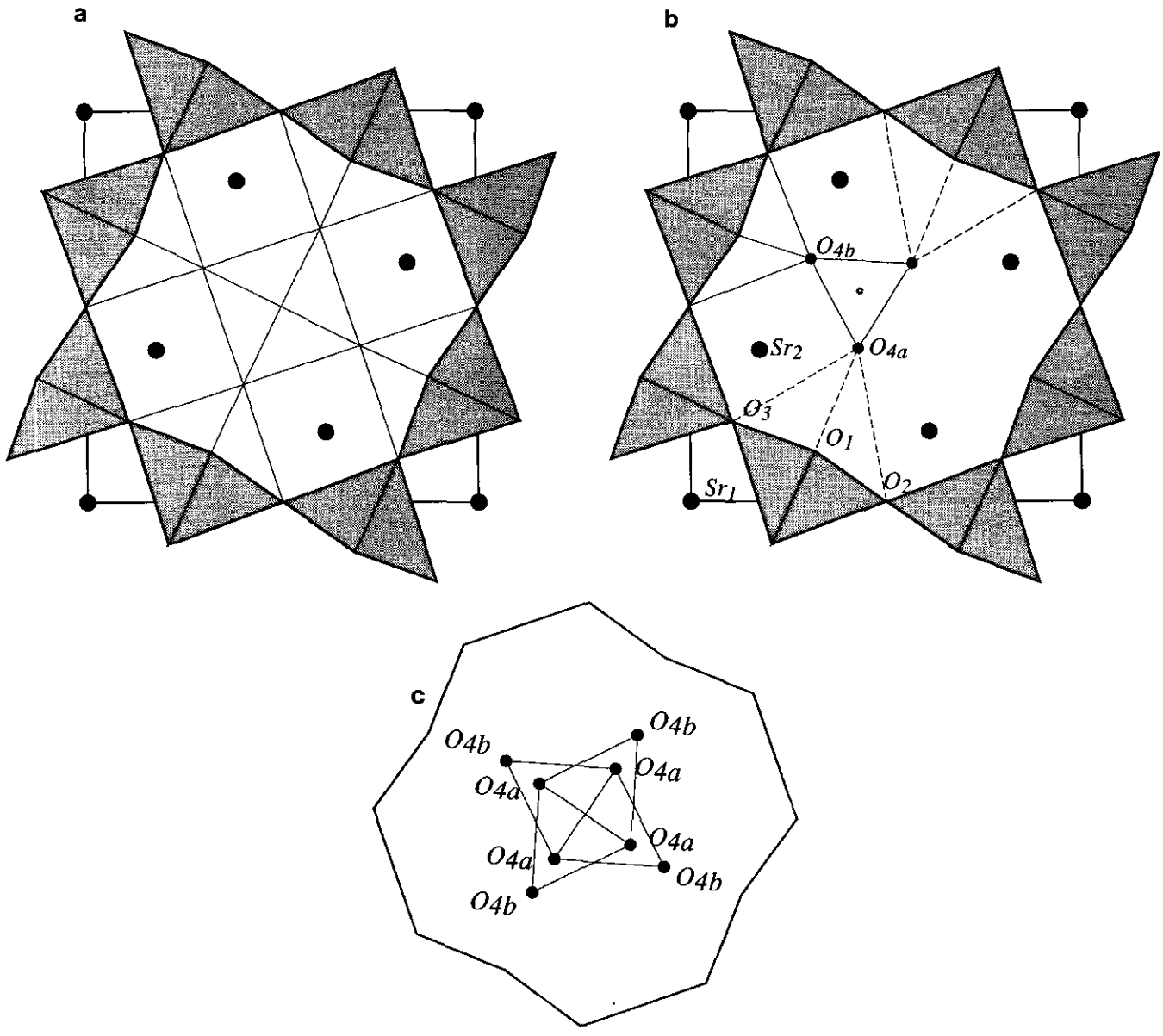

FIG. 7. (a) Model for $Sr_5Mn_4O_{10}$ showing the related perovskite structure. (b) Model for $Sr_5Mn_4CO_3O_{10}$ showing one carbonate group and the manganese coordinations. (c) The four possible orientations of the carbonate groups.

exhibit eight neighbors located at 2.80 Å and four at 3.00 Å. The strontium ions Sr_2, characterized by a tricapped trigonal prismatic coordination, exhibit four oxygen neighbors (O_2, O_3), at distances ranging from 2.57 to 2.65 Å, and two oxygen atoms (O_{4a} or O_{4b}), at distances ranging from 2.68 to 3.10 Å. These six oxygen atoms form the distorted trigonal prism; this prism is capped by three additional oxygen atoms, O_1 at distances ranging from 2.59 to 2.77 Å.

EXTENDED DEFECTS: HREM STUDY

Most of the crystals show a very neat contrast with a well-ordered arrangement of carbonate groups. Nevertheless, two types of defects have been encountered.

The first one deals with the formation of perovskite domains. Frequently, some small domains on the edge of crystals do not show any contrast characteristic of carbonate groups but only a perovskite-type arrangement of dots (Fig. 8a). They can also be observed as isolated defects in a perfect $Sr_5Mn_4CO_3O_{10}$ matrix (Fig. 8b). The crystal image in Fig. 9 shows two domains translated by $\frac{1}{5}(2\mathbf{a} + \mathbf{b})$. The boundary, though coherent, is not planar. The observed contrast on the thin edge of the crystal allows us to propose a model for the boundary (Fig. 9b). It is ensured through a new arrangement of CO_3 groups substituted for MnO_x polyhedra, one every 6 polyhedra

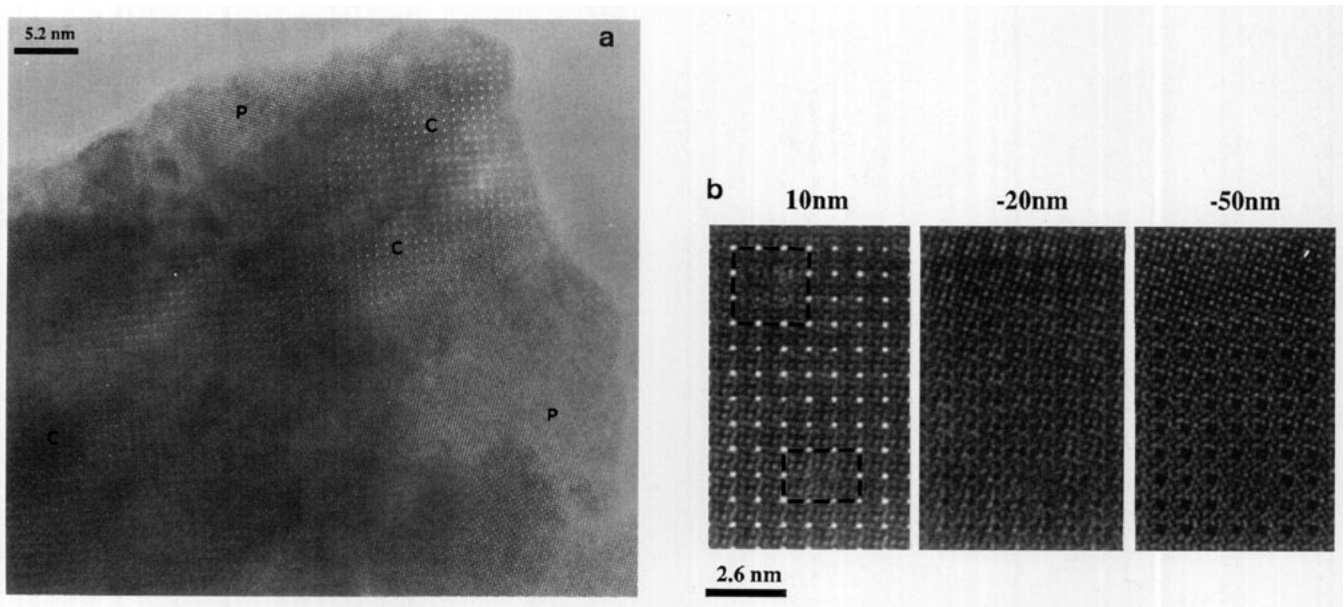

FIG. 8. (a) Medium magnification (001) high-resolution image (focus close to 10 nm) showing $Sr_5Mn_4CO_3O_{10}$-type domains (C) and on the edge of the crystal perovskite-type domains (P). (b) (001) high-resolution images, obtained for three focus values of a crystal showing two isolated perovskite-type defects in a $Sr_5Mn_4CO_3O_{10}$ matrix (circled on 10 nm focus image).

along $\mathbf{a}_P$ and one every 3 polyhedra along $\mathbf{b}_P$, instead of one every 5 along both directions of the perovskite in the $Sr_5Mn_4CO_3O_{10}$ matrix. These observations clearly establish the existence of the $SrMnO_3$ perovskite and of the oxycarbonate $Sr_5Mn_4CO_3O_{10}$ in the same matrix and suggest the possible existence of a large homogeneity range, corresponding to the generic formula $SrMn_{1-x}(CO_3)_xO_{2.5-x/2}$. In such oxides the rows of CO_3 groups and MnO_6 octahedra could be distributed either in an ordered way leading to the formation of microphases or at random. This explains the residual at 1/2, 1/2, 1/2, which corresponds to the local replacement of one row of carbonate groups by one row of MnO_6 octahedra.

The second defect deals with the direction of ordering of the carbonate groups. As already stated above, some slightly rotated domains had been detected by electron diffraction and the corresponding image would show nice Moiré contrast at the superimposition of the slightly rotated domains. In Fig. 10, the electron diffraction pattern can be easily decomposed into two sets of (001) patterns,

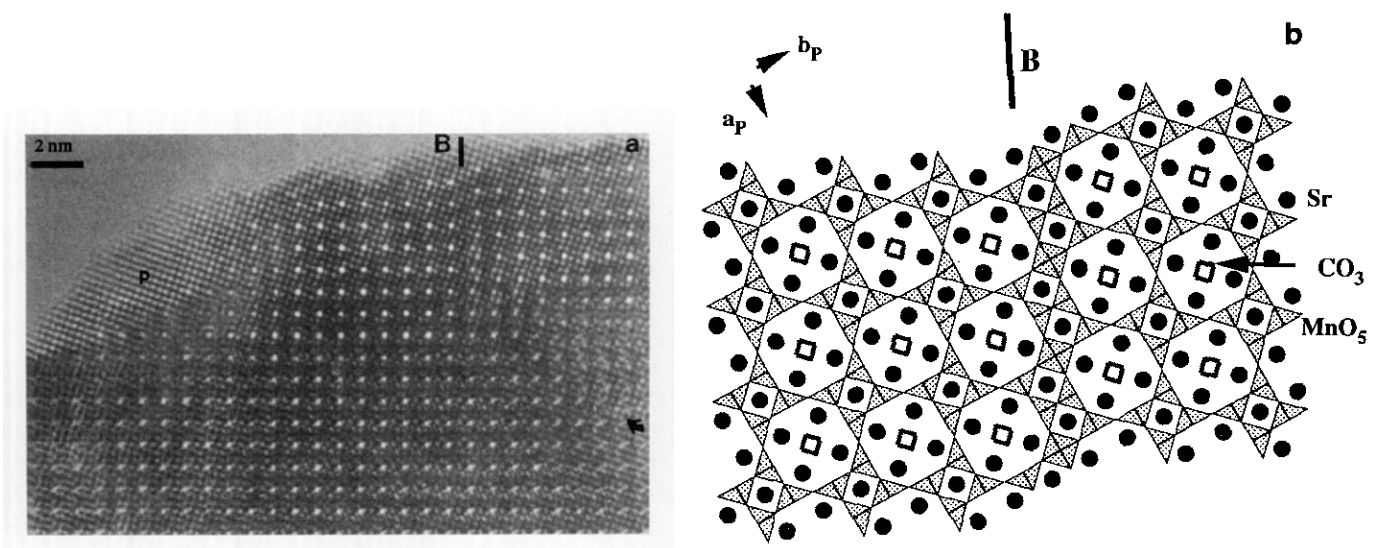

FIG. 9. (a) (001) high-resolution image (focus close to 10 nm) of a crystal showing two translated $Sr_5Mn_4CO_3O_{10}$ domains. The coherent boundary is not planar (B, arrowed). Notice on the edge a perovskite-type domain (P). (b) Schematic model showing that such a boundary can be ensured through MnO_5 pyramids and MnO_6 octahedra.

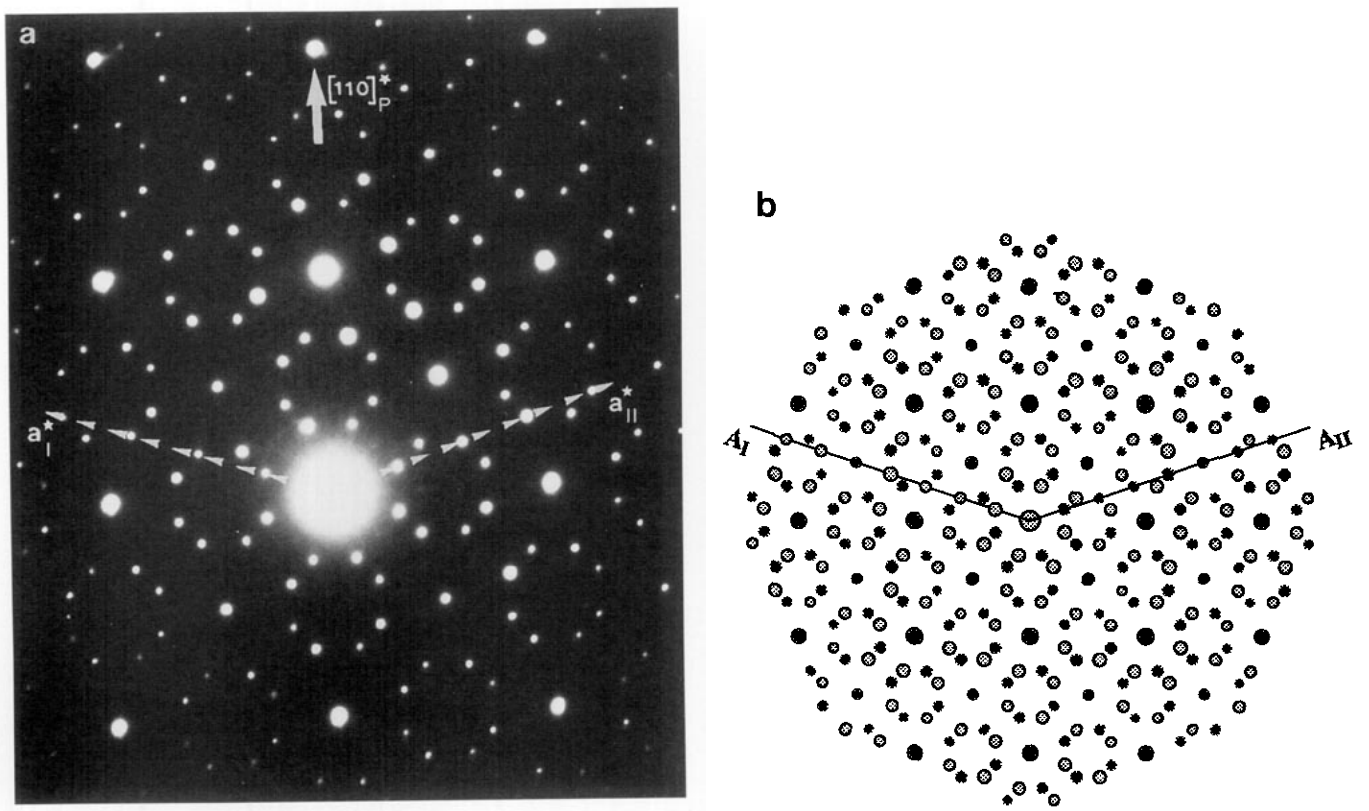

FIG. 10. (001) E.D. pattern (a) and corresponding schematic drawing (b) which can be interpreted through the superimposition of two twinning domains.

the A_I direction being parallel to the [210]* direction of the perovskite subcell and the A_{II} direction of the second domain being parallel to the [120]* equivalent direction of the subcell. Two domains are twinned through the $(110)_P$ perovskite plane. The corresponding high-resolution image confirms this interpretation (Fig. 11). The boundary is not planar but stays almost parallel to the $(110)_P$ twinning plane. The focus value close to 10 nm has been chosen as it allows us to image the superlattice formed at the superimposition of both domains along **c** on the thicker region of the crystal. Indeed, the schematic projection of both domains shows that their superimposition leads to a 2-nm ($5 \times a_P$) square superlattice. Finally, on the edges of the crystals one sometimes observes several rows of oxycarbonates forming ribbons parallel to $(100)_P$ (Fig. 12a), in a similar way to $Sr_2CuO_2CO_3$-type (1, 3) or $YBa_2Cu_2CO_3O_{11}$-type structures (8–10), as schematized, for instance, in Fig. 12b.

MAGNETIC PROPERTIES AND MÖSSBAUER SPECTROSCOPY

The magnetic susceptibility was measured between 80 and 900 K with the Faraday method in an applied field of about 3000 G. The inverse molar magnetic susceptibility of $Sr_5Mn_4CO_3O_{10}$ (Fig. 13) reveals an antiferromagnetic behavior with $T_N = 260(10)$ K. The linear part of the $1/\chi$ versus temperature, fitted with a Curie–Weiss law $\chi = \chi_0 + C/(T - \theta_p)$, leads to a paramagnetic temperature $\theta_p = 140(5)$ K, typical of antiferromagnetic behavior. The effective moment $P_{eff} = 5.09$, deduced from the Curie constant C, is in good agreement with the theoretical value for the Mn^{III} ($P_{eff} = 4.9$). Above 800 K, one observes a loss of weight which is related to the loss of carbon dioxide by the sample.

In order to check the possibility of the existence of two distinct sites—pyramidal and octahedral—for manganese, a Mössbauer spectroscopy study has been undertaken. A sample, doped with about 1% ^{57}Fe, was prepared with the same experimental procedure as the undoped sample. The Mössbauer resonance pattern was obtained in a transmission geometry with a constant acceleration spectrometer using ^{57}Co source held at room temperature. The powder sample was studied at room temperature. A large and symmetric doublet is observed (Fig. 14). Nevertheless the result of the refinement shows that a second doublet exists in a small proportion. The main site is characterized by a large quadrupole splitting: QS = 1.52 mm/s (Table 3). This

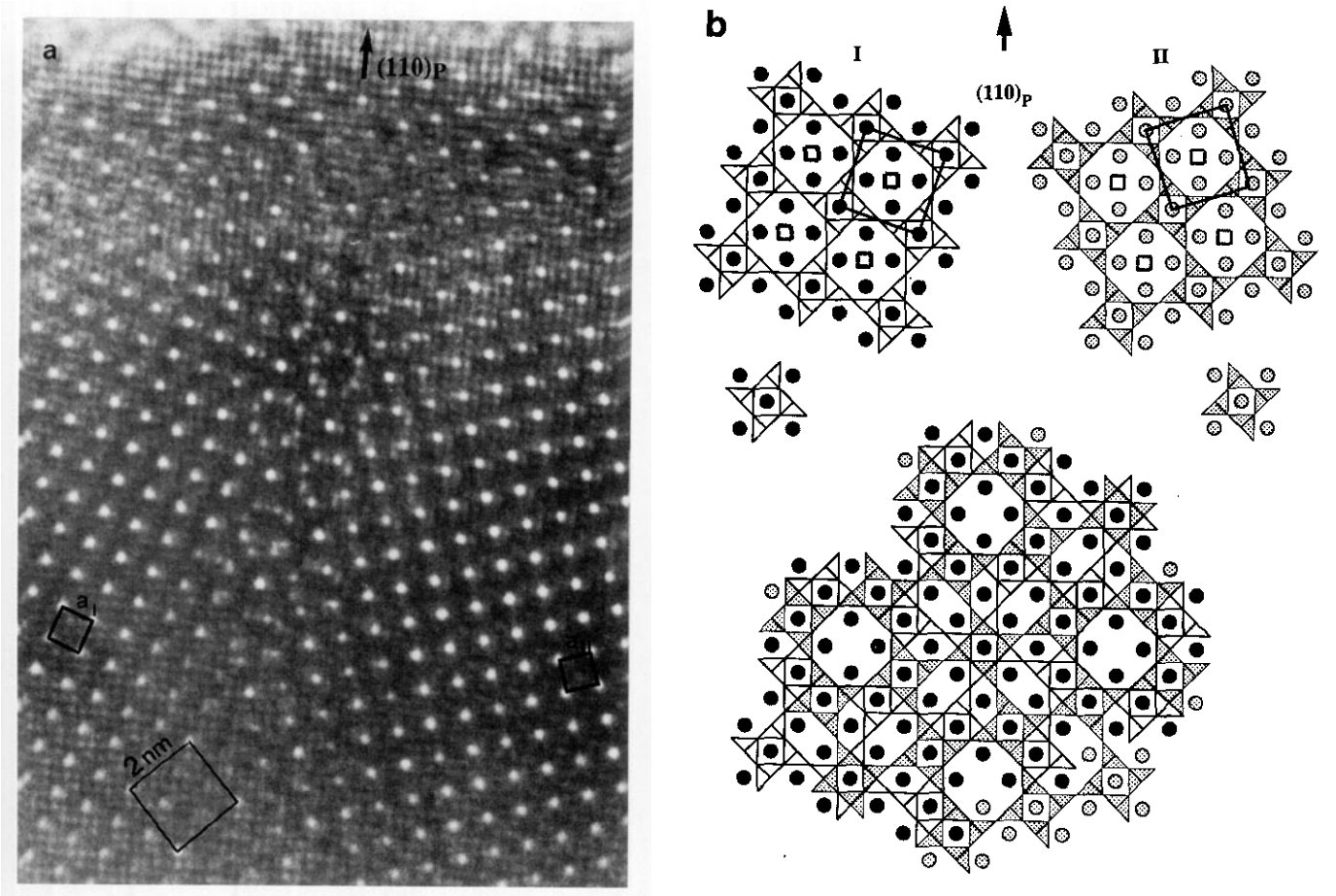

FIG. 11. (a) Corresponding high resolution image of the two twinning domains which share a coherent boundary almost parallel to $(110)_P$ and nearly 3 nm wide (focus close to 10 nm). The observed contrast at the superimposition of both domains follows a 1.96-nm-square periodicity. (b) Schematic explanatory drawing of the formation principle of the twinning boundary. Carbonate groups are omitted at the superimposition of twinning domains.

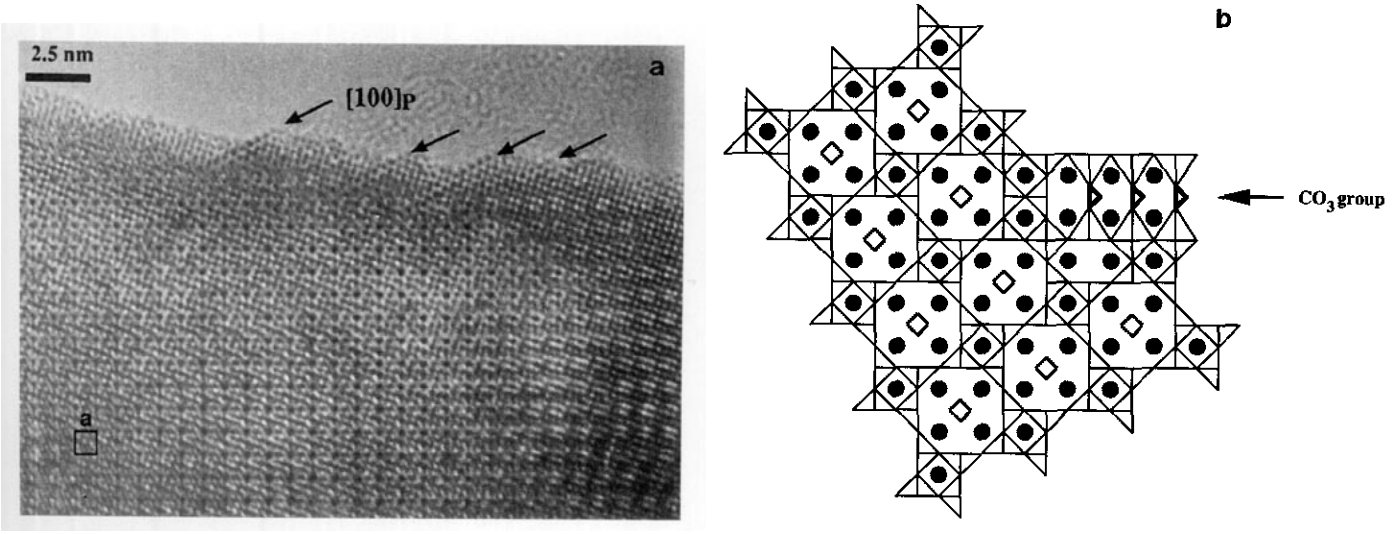

FIG. 12. (a) High-resolution (001) image (focus close to −20 nm) showing on the edge of the crystal ribbons parallel to $[100]_P$ of dark dots. (b) Schematic interpretative drawing of the edge of such a crystal showing rows of carbonate groups.

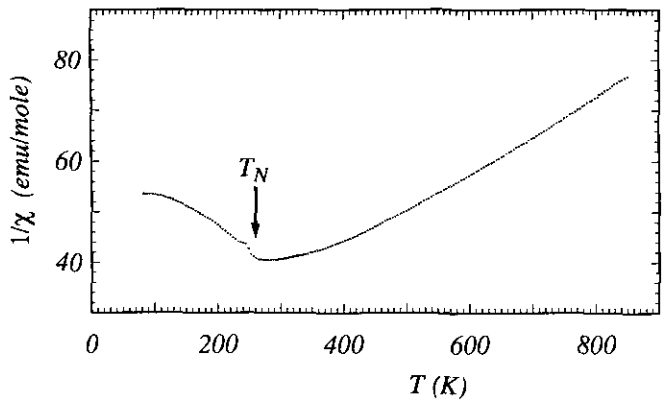

FIG. 13. Inverse magnetic susceptibility of $Sr_5Mn_4CO_3O_{10}$.

value is similar to the quadrupole splitting observed when manganese is substituted by iron in $Sr_2Mn_2O_5$ (13); in this compound, manganese is in a pyramidal coordination and substituted iron has a QS value equal to 1.42 mm/s.

The second doublet, that is about 10% in intensity, is characterized by a QS of about 0.9 mm/s which is compatible with a distorted octahedral coordination. Nevertheless the proportion of weakly distorted coordination for manganese should be 25% according to the XRD results. This can be explained by the fact that Fe^{III} may occupy preferentially the pyramidal sites rather than the octahedral sites. Of course, the second weak doublet might also be produced by a parasitic phase due to an incomplete substitution of manganese by iron. Thus, the Mössbauer study is in agreement with a pyramidal and octahedral configuration but does not prove definitely the existence of an octahedral coordination.

CONCLUSION

A manganese oxycarbonate with a structure closely related to that of perovskite has been isolated for the first time. This study shows the similar behavior of Mn^{III} and Cu^{II}, in agreement with their Jahn–Teller properties that allow a great flexibility of the oxide frameworks in which they are engaged. Nevertheless the oxycarbonate $Sr_5Mn_4CO_3O_{10}$ differs from the copper oxycarbonates synthesized to date by the tridimensional character of the Mn–O framework. The HREM study shows that complex nonstoichiometry phenomena are involved. They should allow mixed valent $Mn^{III} - Mn^{IV}$ oxycarbonates, such as $SrMn_{1-x}(CO_3)_xO_{2.5-x/2+\delta}$, to be generated. A systematic exploration of these oxycarbonate systems will be performed.

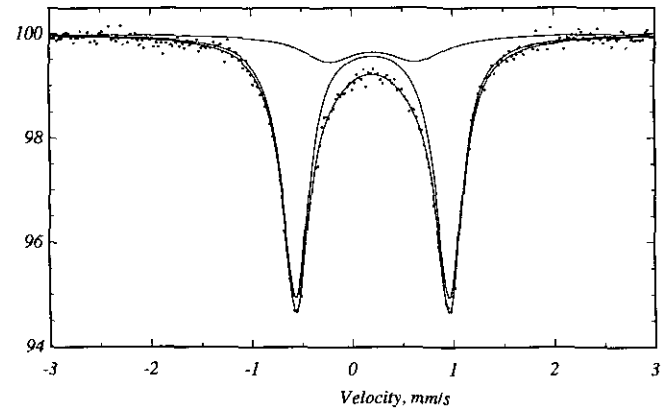

FIG. 14. Room temperature ^{57}Fe Mössbauer spectra of $Sr_5Mn_4CO_3O_{10}$.

TABLE 3
Mössbauer Parameters for $Sr_5Mn_4CO_3O_{10}$ at Room Temperature

IS (mm/s)	Γ (mm/s)	QS (mm/s)	Percentage
0.314	0.16	1.52	90
0.334	0.33	0.87	10

Note. Isomer shift is referred to α-Fe at room temperature.

ACKNOWLEDGMENT

We thank Dr. F. Mauge for assistance in collecting the IR data.

REFERENCES

1. D. V. Fomichev, A. L. Kharlanov, E. V. Antipov, and L. M. Kovba, *Superconductivity* **3,** 107 (1990).
2. K. Kinoshita and T. Yamada, *Nature* **357,** 312 (1992).
3. C. Greaves and P. R. Slater, *J. Mater. Chem.* **1,** 17 (1991).
4. M. Hervieu, C. Michel, G. Van Tendeloo, A. Maignan, C. Martin, and B. Raveau, *Physica C* **235–240,** 25 (1994).
5. D. Pelloquin, M. Hervieu, C. Michel, A. Maignan, and B. Raveau, *Physica C* **227,** 215 (1994).
6. C. Martin, M. Hervieu, M. Huve, C. Michel, A. Maignan, G. Van Tandeloo, and B. Raveau, *Physica C* **222,** 19 (1994).
7. F. Goutenoire, M. Hervieu, A. Maignan, C. Michel, C. Martin, and B. Ravau, *Physica C* **210,** 359 (1993).
8. Y. Miasaki, H. Yamane, N. Ohnishi, T. Kajitani, K. Hirada, Y. Morii, S. Funahashi, and T. Hirai, *Physica C* **208,** 116 (1993).
9. B. Domengès, Ph. Boullay, M. Hervieu, and B. Raveau, *J. Solid State Chem.* **108,** 219 (1994).
10. Ph. Boullay, B. Domengès, M. Hervieu, and B. Raveau, *Chem. Mater.* **5,** 1683 (1993).
11. J. Rodriguez-Carvajal, *in* "Satellite Meeting on Powder Diffraction, Abstracts of the XVth Conference of the International Union of Crystallography, Toulouse, 1990," p. 127.
12. C. Michel, L. Er-Rakho, M. Hervieu, J. Pannetier, and B. Raveau, *J. Solid State Chem.* **68,** 143 (1987).
13. V. Caignaert, M. Hervieu, B. Raveau, and J. M. Greneche, *Chemica Scripta* **27,** 289 (1987).